Femtosecond vibrational dynamics in water nano-droplets

Cringus, Gheorghe Dan

Chapter 3

Ultrafast Anisotropy Dynamics of Water Molecules Dissolved in Acetonitrile

Infrared pump-probe experiments are performed on isolated H_2O molecules diluted in acetonitrile in the spectral region of the OH stretching vibration. The large separation between water molecules excludes intermolecular interactions, while acetonitrile as a solvent provides substantial hydrogen bonding. Intramolecular coupling between symmetric and asymmetric modes results in the anisotropy decay to the frequency-dependent values of ~0-0.2 with a 0.2 ps time constant. The experimental data are consistent with a theoretical model that includes intramolecular coupling, anharmonicity, and environmental fluctuations. Our results demonstrate that intramolecular processes are essential for the H_2O stretching mode relaxation and therefore can compete with the intermolecular energy transfer in bulk water.

This chapter is based on the following papers:

D. Cringus, T.l.C. Jansen, M.S. Pshenichnikov, D.A. Wiersma, "Ultrafast anisotropy dynamics of water molecules dissolved in acetonitrile", J. Chem. Phys. **127** (2007) pp. 084507-1 – 084507-11.

D. Cringus, T.l.C. Jansen, M.S. Pshenichnikov, D.A. Wiersma, "Ultrafast intramolecular energy transfer in water", in Ultrafast Phenomena XV, Eds: P. Corkum, D. Jonas, D. Miller, A.M. Weiner, Springer-Verlag, Berlin (2007) pp. 439-441.

3.1 Introduction

Liquid water is an essential substance that plays a large variety of unique roles in biochemical processes due to its peculiar properties. For instance, water ensures the stabilization and functionality of biological structures[3], facilitates the proton and electron transfer between proteins [4], and mediates binding interactions between biomolecules [5].

Most of the unique properties of water are related to the network of strong three-dimensional (3D) hydrogen bonds that interconnect the water molecules [6,7]. In the last years, the advances in laser technology, namely in the generation of ultrafast IR pulses [8-12], made it possible to monitor processes that occur on time scales as short as 100 fs. Such experiments opened new perspectives on the investigation of the structure [2] and dynamics of the hydrogen bond network in liquid water [13-16].

The complexity of liquid water properties calls for simplifying approaches which are able to reveal different aspects of the physics involved. One direction that has been conventionally pursued is the removal of the complications related to the intra- and intermolecular couplings between the OH oscillators by substitution H_2O with its deuterated isotope HDO [2,13,14,17]. Another possibility, which also mimics biological situations [18], is to alter the complexity of the hydrogen bond network by studying water at interfaces [19,20], in reverse micelles [21-28], or in mixtures with various solvents [2,29,30]. The last setting is particularly advantageous because it allows investigating spatially separated water molecules and, thus, provides a unique opportunity to study purely intramolecular properties, which are not screened by interactions with other water molecules. In addition, by a careful choice of solvents with different hydrophilic characters, the influence of the surrounding on the water molecule can be investigated in a progressive manner, from weakly hydrogen-bonded situations [29,30] to rather strongly bonding environments [2,29,30].

An interesting model system, which comprises both hydrogen bonded and free hydroxyl groups, can be obtained by dissolving water in a mixture of acetone and carbon tetrachloride (CCl_4) [31]. From IR pump-probe measurements it has been concluded that the ultrafast dynamics in such a ternary mixture reflect breakage and reformation of the hydrogen bonds [31]. In contrast to bulk water, where a dangling hydrogen bond has been convincingly shown to be a transition state[14], in water/acetone/carbontetrachloride mixtures the doubly bonded configuration was argued to live very shortly and to decay rapidly (at a 100 fs time scale) into a single-bonded state[31]. However, the complexity of the ternary mixture makes the interpretation of spectroscopic data quite difficult as some processes, for instance, intramolecular couplings, might be concealed.

A reasonable compromise between the hydrogen bond strength and hydrophilic properties of the solvent is offered by acetonitrile [2,32,33]. The hydrogen bonds formed between water and acetonitrile are much weaker than the water-water hydrogen bonds. Nevertheless, they considerably improve the miscibility of the two liquids, allowing them to mix in any ratio. Moreover, MD simulations have shown that at higher concentration the water molecules tend to form clusters surrounded by the solvent[32-35]. Thus, in such mixtures the complexity of the water aggregates can be varied in a controlled way, from monomers to bulk, by simply adjusting the concentration [2]. These systems can therefore provide the link between bulk water with an extensive 3D hydrogen bond network and water molecules in weakly hydrogen-bonding solvents [29,30]. In early IR pump-probe experiments on water dissolved in acetonitrile, the characteristic time for the symmetric-asymmetric mode energy exchange was estimated below 1.5 ps [30] but a more accurate determination was not possible because of the limited time resolution.

A good comprehension of the dynamics of an isolated water molecule dissolved in acetonitrile, as well as the water-solvent interactions, is required as a first step toward the understanding of the more complex situation of water clusters. Namely, the structural variety of the hydrogen-bonded complexes formed around a single water molecule and their influence on the spectroscopic observables should be elucidated. Furthermore, the percentage and persistency of broken hydrogen bonds in this particular liquid matrix need to be revealed. Finally, an important issue concerns the vibrational delocalization and intramolecular energy redistribution, which are characteristic only of the H_2O molecule and not of its HDO isotopomer because of the substantial coupling of the two OH oscillators.

In this paper we report Fourier transform infrared (FTIR) and IR pump-probe experiments with 100 fs time resolution performed on the OH stretching modes of water dissolved in acetonitrile. The low concentration of water molecules ensures that there are no intermolecular water interactions, and therefore all observed dynamics are due to response of well-separated water molecules. By spectrally resolving the nonlinear signal after an ultrafast IR excitation and use of polarization selectivity, we a reveal rather complicated intramolecular dynamics and a rapid decay of anisotropy. The underlying phenomena behind the experimental observations are confirmed by numerical modeling, which is in good agreement with the experiments. Our results show that intramolecular processes play a crucial role in the subpicosecond water dynamics and strongly suggest that these processes could compete with the intermolecular energy transfer in bulk water [12,36].

3.2 Experimental

The experiments were performed with broadband [bandwidth ~200 cm^{-1} full width at half maximum (FWHM)] 70-fs pulses centered at 3550 cm^{-1} and generated by a home-built optical parametrical amplifier [9]. The pump and probe beams, with an intensity ratio of 10:1, were focused in the sample volume and then recollimated by spherical mirrors. Subsequently, the probe beam was dispersed through a monochromator to follow the dynamics at any selected frequency between 3325 and 3675 cm^{-1}. A synchronous 500 Hz chopper was inserted into the pump beam to provide lock-in detection by an InSb diode or a 64 elements mercury cadmium telluride (MCT) array. The spectral width of the mid-IR pulses ensured a uniform excitation of the water OH stretching vibration and allowed a simultaneous detection of population differences on both fundamental and first overtone transitions. The polarization of the probe beam was set at 45^{o} with respect to the pump beam, while a polarizer installed after the sample selected either the parallel or the perpendicular component of the probe beam for detection. The isotropic (also known as rotation-free) and anisotropic signals were then calculated from the two orthogonally polarized probe scans [37]. The sample, consisting of H_2O dissolved in acetonitrile with a molar ratio of ~0.017, was contained in a 100 μm thick freestanding jet, resulting in a maximum optical density at the OH stretching frequency range of ~0.5. Pump-probe experiments performed on neat acetonitrile revealed no substantial nonresonant solvent contribution. In order to diminish the absorption by water vapors in the ambient air, the region traveled by the mid-IR beam was purged with nitrogen.

The virtually impulsive excitation of the entire stretching region ensured that spectral diffusion does not affect the experimental transients. Nonetheless, the pump-probe data within ±100 fs around zero delay should be read cautiously as they might be distorted by coherent coupling between the pump and probe pulses. Interestingly enough, the short time anisotropy does not seem to be significantly affected, most probably because of identical scaling of nonlinear response functions for parallel and orthogonal polarizations corresponding to Feynman diagrams of "wrong" pulse sequences [38].

3.3 Results

The vibrations of an isolated water molecule consist of combinations of three fundamental modes, and thus each vibrational state is described by three quantum numbers $|n_s n_b n_a>$ associated with the symmetric stretch, bend, and asymmetric stretch of the H–O–H bonds, respectively [39]. The research presented here involves only the fundamental and the first

excited states of the symmetric and asymmetric stretching modes, i.e., $|n_s 0 n_a>$ levels, where n_s, $n_a = 0, 1, 2$ (Fig. 3.1). It should be pointed out that strictly speaking, the eigenmode representation is not accurate for describing the water molecule dissolved in acetonitrile as, first, the system is essentially anharmonic and, second, both modes are dynamically broadened due to the environmental perturbations. However, we will use this terminology for the sake of simplicity keeping in mind the above outlined reservations.

In order to understand the microscopic structure of the sample, the types of hydrogen bonds in which the water molecules are involved need to be clarified. It is well known from both calculations [32-35] and experiments [2] that in water-acetonitrile mixtures the water molecules tend to cluster (the so-called effect of microheterogeneity). However, this process occurs only when the water/acetonitrile molar ratio exceeds a certain value, typically 0.1 [34]. In our experiments, the water concentration was considerably below this value, and therefore the sample contained only isolated water molecules trapped in an acetonitrile matrix. Figure 3.2(a) shows the absorbance profiles in the OH stretching region for the samples containing H_2O (solid curve), isotopically substituted HDO (dashed curve), and neat acetonitrile (dotted curve). With the exception of the two week lines located at 3619 and 3655 cm^{-1}, the neat acetonitrile spectrum is free of absorption in the spectral region of interest, i.e., from 3300 to 3800 cm^{-1}.

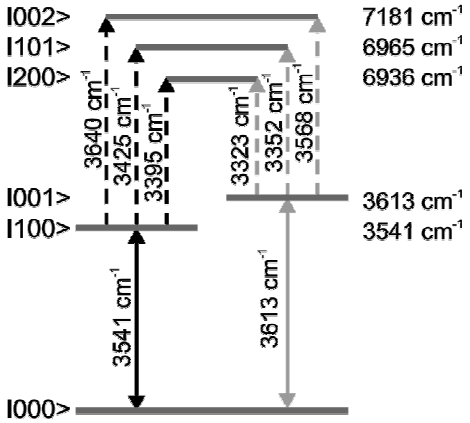

Figure 3.1. Schematics of the H_2O stretching modes and transitions relevant for pump-probe experiments. The notation $|n_s n_b n_a>$ stands for three quantum numbers associated with the symmetric stretch, bend, and asymmetric stretch of the H–O–H molecule, respectively. The bending mode has no relevance to the presented experiments. The energies of transitions and level assignments are the results of calculations.

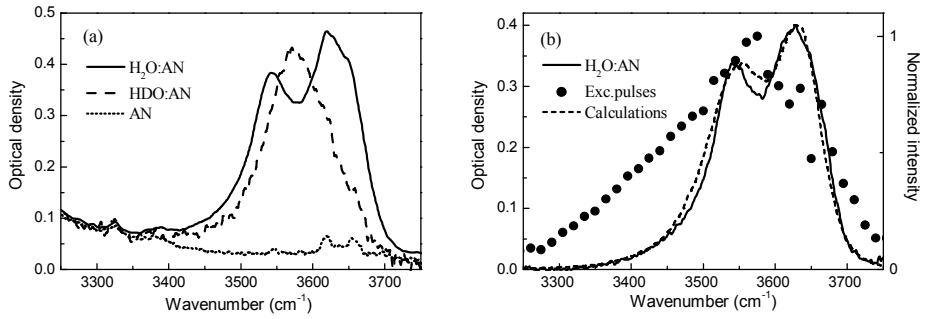

Figure 3.2. (a) Absorption spectra of H_2O (solid) and HDO (dashed) molecules dissolved in acetonitrile (dotted curve). In (b), the H_2O spectrum is corrected for the solvent contribution. The excitation pulse spectrum is shown by solid dots. The dashed curve depicts the simulated absorption spectrum.

We begin our consideration with the analysis of isotopically substituted water (HDO) dissolved in acetonitrile. In contrast to the H_2O molecule, the OH and OD oscillators have different frequencies and are therefore effectively decoupled. In this case, the OH stretching band consists of a single slightly asymmetric peak centered at ~3575 cm^{-1} with an ~85 cm^{-1} width FWHM [Fig. 3.2(a), dashed curve]. On the one hand, this absorption line is noticeably blue-shifted and narrowed compared to the HDO in D_2O case [2,40-42]. On the other hand, it is situated at much lower frequencies and is substantially broader than in the case of HDO in nonpolar solvents [2]. This proves that water and acetonitrile form hydrogen bonds of the type O–H· · ·N, which are nevertheless on average much weaker than the O–H · · · O bonds formed in bulk water. No signature of nonbonded OH groups [30,31,43], which would appear as a narrow peak between 3600 and 3700 cm^{-1}, is present in the spectrum. Thus, the most stable configuration is reached when the hydrogen atom of the water molecule is involved in a hydrogen bond with the nitrogen atom of acetonitrile. The preference of a water molecule to form two hydrogen bonds has been predicted by theoretical calculation [32]. Also, as can be seen from Fig. 12(a) of Ref. [33], water molecules in water-acetonitrille mixtures donate on average ~1.8 hydrogen bonds, and this number remains practically unchanged with the decrease of the water concentration to about 5% – 10%. The results of recent two dimensional (2D) IR measurements on HDO in acetonitrile [44,45] are also consistent with this microscopic picture as they do not show any spectral or dynamical features that might be associated with dangling OH oscillators [11,14,46]. Thus, we can conclude that the contribution of nonbonded hydroxyl groups – if any – to the experimental observables is negligibly small. Although the water oxygen also

forms hydrogen bonds with the hydrogen atoms of neighboring acetonitrile [35], these have a much smaller influence on the OH stretching band, contributing only slightly to the line broadening but not generating any additional line splitting [42,47].

A similar hydrogen bond arrangement, with both H atoms of water molecules linked by O–H · · · N bonds to nitrogen atoms, is to be expected when H_2O is dissolved in acetonitrile. Therefore, the symmetry in this case resembles the C_{2v} symmetry of the isolated H_2O molecule, with the inherent perturbations introduced by the fluctuating environment. Due to this configuration, the stretching vibration is delocalized over the water molecule to produce symmetric (|100>) and asymmetric (|001>) modes. The corresponding fundamental transitions are easily identified in the absorption spectrum [Fig. 3.2(b), solid line]: |000> → |100> has a central frequency of ~3545 cm^{-1} and |000> → |001> is centered at 3630 cm^{-1}. Again, no spectral signature of nonbonded OH groups is evident from the spectrum. It is interesting to note that what appears to be the stable and predominant conformation in the water/acetonitrile mixture has previously been considered as a rare and shortly lived state in water/acetone/CCl_4 mixtures [31].

In the pump-probe experiment, an intense and broadband [Fig. 3.2(b), dots] pump pulse simultaneously excites both the symmetric |100> and asymmetric |001> stretching

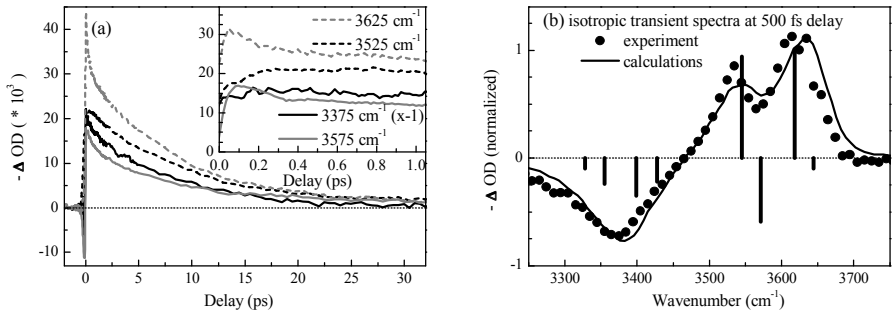

Figure 3.3. (a) Isotropic transients at several representative frequencies and (b) isotropic transient spectra at 500 fs delay. The inset in (a) shows transients for orthogonal pump and probe polarizations. The transients in (a) are obtained around the central frequencies of the symmetric (3525 cm^{-1}, black dashed) and asymmetric (3625 cm^{-1}, gray dashed) modes, near the |001> → |002> transition (3575 cm^{-1}, gray solid), and at the maximum of the induced absorption (3375 cm^{-1}, black solid, the sign is reversed). Vertical lines in (b) show positions and intensities of the transitions contributing to the pump-probe signal. In (b), the dots show the experimental and the solid curve the calculated isotropic pump-probe spectra at a 500 fs delay.

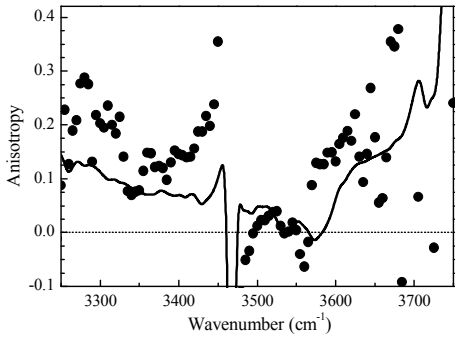

Figure 3.4. Experimental (dots) and simulated (solid curve) transient anisotropy spectra at a 500 fs delay. Note the decrease of anisotropy to 0-0.2 values within the first 500 fs for most frequencies. The breaking point around 3470 cm^{-1} is due to the zero amplitude of the isotropic transient spectrum at this frequency [Fig. 3.3(b)].

modes. At delays longer than 2 ps, the rotation-free transients [Fig. 3.3(a)] are well fitted by a monoexponential function with 8 ± 0.5 ps time constant, which is attributed to the lifetime of the OH stretching mode of a water molecule in acetonitrile. This assignment is also supported by the similarity of this value with the 12 ps relaxation time of the OH stretching mode of HDO dissolved in acetonitrile [2]. It is still unclear whether the stretch relaxation involves energy transfer to the bending mode, as in bulk water [48-50], or to vibrational states of the solvent, as has been shown for the bending mode of monomeric water [51]. The substantially smaller detuning of the bend overtone from the stretching modes for H_2O as compared to HDO (~350 versus ~700 cm^{-1}, respectively) points toward the former scenario. Regardless of the precise relaxation pathways, the somewhat shorter lifetime found in the case of H_2O can be qualitatively explained by the broader absorption line, which improves the resonance with the accepting mode(s).

At short delay times, the transients exhibit a strong dependence on the frequency. This becomes clearer when the pump-probe transients with orthogonal polarizations are considered [Fig. 3.3(a), inset]. For instance, at 3625 cm^{-1}, close to the peak of the asymmetric stretch absorption, the signal decays by ~20% of the maximum value within 0.5 ps (gray dashed curve), while near the center frequency of the symmetric stretch at 3525 cm^{-1}, the signal increases at a similar time scale (black dashed curve). In both cases, the initial relaxation/growth occurs with a similar time constant 0.2 ± 0.05 ps. In contrast, at the maximum of induced absorption at 3375 cm^{-1} hardly any dynamics different from the population kinetics are visible (solid line in Fig. 3.3(a), inset).

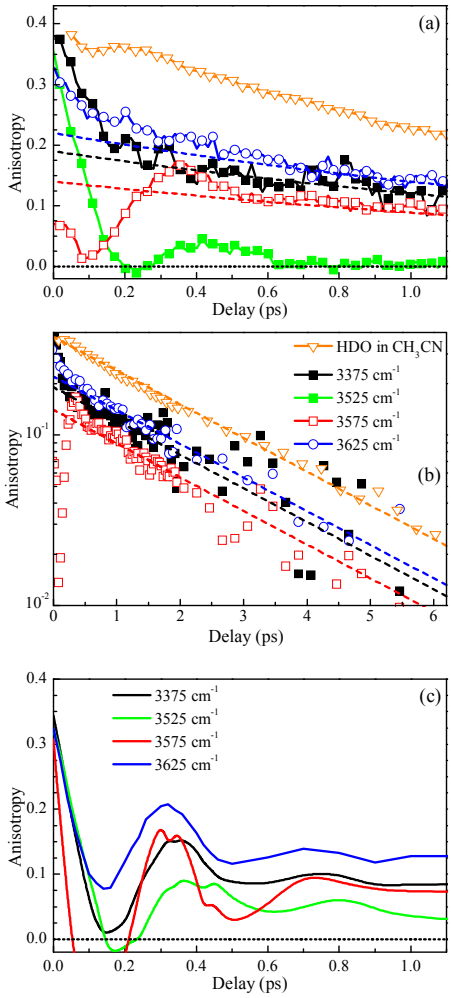

Figure 3.5. Transient anisotropies at the same frequencies as in Fig. 3.3(a): experimental transients at (a) short and (b) long delays, and (c) calculations. The orange triangles in (a) and (b) show the HDO in acetonitrile data measured at 3550 cm^{-1}, i.e. near the absorption maximum; the rest of the transients are for H_2O in acetonitrile. The lines in (a) and (b) show a monoexponential fit to the experimental data at long delays with the 2.2 ps time constant that reflects the true rotational anisotropy decay. This process is not included in simulations (c).

The isotropic transient spectrum at a 500 fs delay between pump and probe is shown in Fig. 3.3(b) as solid dots. Bleaching and stimulated emission at the lower transitions are clearly identified by the two positive peaks that appear around the fundamental frequencies. In contrast, the excited state absorption is much more complex and difficult to interpret, as it comprises six different frequencies, corresponding to the transitions between the singly excited (|100> and |001>) and doubly excited (|200>, |002> and |101>) states (Fig. 3.1). It is also obvious that the gap between the |000>→|100> and |000>→|001> ground-state transitions is somewhat deeper than that at the linear absorption spectrum. This hints to the conclusion that at least one of the transitions to the double-excited states lies in between the two fundamentals. The same transition also causes a small shift of the bleaching peaks of the transient absorption spectrum compared to its steady-state counterpart. The other higher-state transitions contribute to the broad featureless band centered around 3370 cm^{-1}. The absence of any noticeable modulation in this band prevents the direct experimental assignment of transition frequencies and therefore requires theoretical modeling (Section 3.4).

Figure 3.4 shows as dots the experimental transient anisotropy spectrum at the 500 fs delay, from which it can be seen that the anisotropy quickly decays to values of 0-0.2 within the first half of a picosecond. A strong anisotropy wavelength dependence is also apparent, with an asymptotic point at ~3470 cm^{-1}, where the anisotropy is infinitely large, and a zero value around 3525 cm^{-1}. The first peculiarity is partly explained by noticing that at that frequency induced absorption is balanced by stimulation emission and bleaching [Fig. 3.3(b)], setting as a result the denominator in the anisotropy fraction at zero. The explanation for the zero anisotropy around 3525 cm^{-1} is not apparent in a conventional framework where the anisotropy decay is interpreted as randomizing of the dipole moment directions due to rotational motions of the molecule. It is very unlikely that the water molecule in – even weakly – hydrogen-bonded systems has this degree of looseness. In addition, the nonzero anisotropy values at other frequencies speak against this hypothesis.

To clarify these issues, the transient anisotropy data at several representative wavelengths are shown in Figs. 3.5(a) and 3.5(b). Again, a comparison with a HDO molecule dissolved in acetonitrile, where the OH and OD oscillators are spectroscopically uncoupled, is proven useful. In the case of HDO, the anisotropy shows a small wiggle at early times (Fig. 3.5(a)) after which it decays monotonically with a ~2.2 ps time constant [Fig. 3.5(b)], reflecting the rotational diffusion. The oscillatory behavior observed at short delays occurs with an initial drop to about 0.35 and a subsequent recurrence with a period of about 240 fs. This behavior closely resembles the anisotropy data on HDO dissolved in D_2O by Loparo et al. [52], suggesting that the initial contribution might reflect modulations in the O–H · · · O hydrogen bond length. Molecular dynamics (MD) simulations [33] on

water-acetonitrile mixtures support this interpretation by predicting a broad resonance band in the bath spectral density around 100 cm^{-1}. If follows from the same MD simulations that the magnitude of spectral density of librations quickly decreases with water concentration, and therefore it is not likely that the librational motion influences the initial anisotropy decay. In any case, the amplitude of the initial component in the measured anisotropy does not exceed 5% – 10% [Fig. 3.5(a)]. This conclusion is also in perfect agreement with recent anisotropy measurements on HDO molecules in weakly hydrogen-bonded environments [31], where it was demonstrated that the anisotropy decays by a mere 10% in the first few hundred femtoseconds.

The anisotropy data on H_2O in acetonitrile show a remarkably different behavior. Despite the fact that the transient anisotropy displays a pronounced frequency dependence, two distinctly different time scales are clearly discernible. The data are well described by biexponential functions with decay times of 0.2 ± 0.1 and 2.2 ± 0.5 ps. The longer time is similar to the value found for the HDO rotational diffusion time. As the only difference in rotational diffusion between the H_2O and HDO molecules can originate from the slightly different momenta of inertia, we can conclude that the 2.2 ps time reflects the rotational diffusion of the H_2O molecule embedded in the acetonitrile matrix.

In contrast to the slow component, the fast decay is unique for the H_2O molecule, as its amplitude is clearly much larger than observed for HDO. For instance, if the long-time rotational decay of 2.2 ps of the 3625 cm^{-1} anisotropy transient is extrapolated to zero delays, a value of ~0.22 is obtained [Figs. 3.5(a) and (b)], which is substantially lower than 0.4 expected for an uncoupled transition. Furthermore, this comparison also shows a much faster initial (up to 0.5 ps) decay of the anisotropy [Fig. 3.5(a)]. At other frequencies where responses of several transitions overlap, the fast part in the anisotropy decay is even more apparent. In particular, at the 3525 cm^{-1} wavelength the anisotropy reaches zero values in 0.2 ps and after a short recurrence remains at this level.

From the considerations above, we can conclude that the fast component in the H_2O anisotropy decay can be explained neither by rotational motions of the molecule, including libration or inertial rotations, nor by some specific water-solvent interactions. Also, the low concentration of water molecules ensures that the OH oscillators belonging to different water molecules do not interact with each other. Hence, the only mechanism left accountable for the observed anisotropy loss at short delays is the interaction of the two *intramolecularly* coupled OH oscillators. Another interesting feature of the transient anisotropy is the peculiar behavior around the wavelength of 3525 cm^{-1}, namely, the underdamped oscillations with a 350-400 fs period. This roughly corresponds to the inverse frequency splitting between the symmetric and asymmetric modes of 80 cm^{-1}.

3.4 Theory

The theoretical approach presented in this section was developed by Dr. Thomas la Cour Jansen from the Center for Theoretical Physics, Zernike Institute for Advanced Materials, University of Groningen, The Netherlands. The method and the specificities of our system are briefly outlined below presented, while a more elaborate description can be found in Ref. [53]. In modeling the pump-probe signals we primarily focus on the first 500 fs when the intramolecular dynamics presumably dominate the system response. Other processes like rotational diffusion (2.2 ps time scale) and population relaxation (8 ps time scale) were not included in the model as they play little roles at the subpicosecond time scale. If needed, these processes can be introduced straightforwardly in a phenomenological way (i.e., multiplying the respective transients by exponential terms). Short time reorientational effects due to librational motion and/or inertial rotation were also shown to be negligibly small (see the previous section) and were therefore excluded from modeling.

The steady-state and transient spectra were calculated from a Hamiltonian trajectory using the numerical integration of the Schrödinger equation [53,54]. In essence, the system was modeled by a time-dependent Hamiltonian, where the vibrations of interest are described quantum mechanically while the surrounding bath is accounted for through the modulation of the frequencies and couplings between the system vibrations. The modulations due to the bath can be obtained either through molecular dynamics simulations or by using a stochastic model along with independent data, for instance, from echo-peak shift measurements [2].

For the OH stretch vibrations of water, the system of interest comprises the two local OH modes and their overtones. These states are described by the standard exciton Hamitonian for simulating 2D IR spectra [55,56],

$$H(t) = \omega_1(t)\ B_1^+ B_1 + \omega_2(t)\ B_2^+ B_2 + J\left(B_1^+ B_2 + B_2^+ B_1\right) - \frac{\Delta}{2}\left(B_1^+ B_1^+ B_1 B_1 + B_2^+ B_2^+ B_2 B_2\right), \qquad (1)$$

where indexes 1 and 2 denote the two local stretch vibrations with the respective time-dependent frequencies ω_1 and ω_2, and J is the coupling between the two. Δ is the anharmonicity of each local stretch vibration, and B_i , B_i^+ ($i = 1, 2$) are the usual Bose creation and annihilation operators.

The oscillator frequencies fluctuate in time due to interactions with the surrounding solvent. The two local OH stretch vibrations are connected through the oxygen atom, giving rise to the splitting into symmetric and asymmetric normal vibrations. The coupling

is largely mechanical, and therefore we assume that it is independent of the solvent, allowing J to be treated as a constant. The anharmonicity Δ is assumed to be independent of the solvent perturbations and is therefore regarded as a constant in time.

The time evolution of the quantum system is then given by the time-dependent Schrödinger equation

$$\frac{\partial}{\partial t}\Psi(t) = -\frac{i}{\eta}H(t)\Psi(t)\,. \tag{2}$$

Here, H is the time-dependent system Hamiltonian given in Eq. 1 and $\Psi(t)$ is the wave function of the vibrational system. The time evolution of the quantum system is found by dividing the Hamiltonian trajectory into short time intervals, during which the Hamiltonian can be approximated to be constant. The wave function $\Psi(t)$ can then be found if its value at an earlier time t_0 and the fluctuating Hamiltonian for the interval between these times are known,

$$\Psi(t) = \mathbf{U}(t,t_0)\Psi(t_0) = \left[\prod_{n=0}^{n=(t-t_0)/\Delta t} e^{-\frac{i}{\eta}H(t_0+n\Delta t)\Delta t}\right]\Psi(t_0)\,, \tag{3}$$

with Δt being the duration of the short time intervals. The time evolution operator $\mathbf{U}(t,t_0)$ determined by this equation is then used in the calculation of the (non)linear response functions [57].

The linear absorption spectrum is given by the Fourier transform of a two-point correlation function of the transition dipole operators, $\boldsymbol{\mu}$,

$$I_{abs}(\omega) = \mathrm{Im}\int_0^\infty dt_1 \frac{i}{\eta}\left\langle \boldsymbol{\mu}(t_1+t_0)\mathbf{U}(t_1+t_0,t_0)\boldsymbol{\mu}(t_0)\right\rangle e^{-i\omega t_1} e^{-t_1/2T_1}\,. \tag{4}$$

The exponentially decaying term accounts for the excited state lifetime T_1, which was set at 1 ps in order to limit the numerical integration span. The spectral shapes are not affected by its precise value as long as it is much longer than the inverse spectral width. The expressions for the third-order response functions giving rise to the transient pump-probe spectra involve four transition dipoles. These are quite complex and are discussed in detail in Ref. [53]. It is, however, important to stress that these expressions treat population transfer and coherent superpositions of the involved states during the waiting time on an equal footing. Nonadiabatic effects during the interval between the two pump pulses and after the probe pulse are accounted for as well. The frequency trajectories were constructed

using a Gaussian random number generator in the following way. For each local mode the generalized coordinate (i.e., the H · · · N distance) was described by a sum of a fast and a slow fluctuating parameter, $x_F(t)$ and $x_S(t)$, respectively. The distributions of the coordinates were restricted to be Gaussian. The coordinate autocorrelation functions were fixed to be biexponential,

$$C(t) = \sigma^2 \cdot \left(A_F e^{-t/T_F} + A_S e^{-t/T_S} \right), \tag{5}$$

were T_F and T_S are the timescales, and A_F and A_S the relative intensities of the two components. The exponential correlation was ensured by constructing each of the fluctuating parameters at one time step as the weighted sum of the same parameter at the previous time step and a random number $G(\sigma)$ from a Gaussian distribution with width σ,

$$x(t + \Delta t) = x(t) \exp(-\Delta t / T) + G\left(\sigma\sqrt{A}\right)\sqrt{1 - \exp(-2\Delta t / T)}\,. \tag{6}$$

Here, T is the time scale and A the relative intensity taken from the biexponential fit. As the absorption spectrum is symmetric due to the nonlinear frequency dependence of the OH mode on the generalized coordinate, we use the following ad hoc connection between the two:

$$\omega_{1,2}(t) = \langle\omega\rangle + \frac{\beta\sigma}{\alpha}\left(1 - e^{-\alpha x_{1,2}(t)/\sigma}\right) \tag{7}$$

with the dimensionless asymmetry parameter α, mean frequency $<\omega>$ and normalization coefficient β. To understand the physical meaning of α, it is instructive to extend Eq. 7 into the Taylor series,

$$\omega_{1,2}(t) = \langle\omega\rangle + \beta \cdot x_{1,2}(t) - \frac{\beta}{2}\frac{\alpha x_{1,2}(t)^2}{\sigma} + \ldots\,. \tag{8}$$

With the asymmetry parameter $\alpha = 0$, the frequency fluctuations are linearly dependent on the coordinate fluctuations, and the spectra are symmetric. This is exactly the approximation of the multimode Browning Oscillator model [57]. The third term in Eq. 8 introduces the quadratic coupling that is proportional to the asymmetry parameter α, etc.

Due to the symmetry considerations, the average frequency of both local OH stretch vibrations is equal to $<\omega>$, while the fluctuation of the two frequencies is presumed to be uncorrelated. This assumption is motivated by the fact that the frequency of the OH stretch

is predominantly determined by the degree of hydrogen bonding to the hydrogen atom, as it has been shown for HOD in D_2O [42]. The hydrogen bonding to the two hydrogen atoms in a water molecule is largely independent [56], and therefore the frequencies of the local OH vibrations are uncorrelated.

A time step of 10 fs was used in the applied generalized stochastic method for the construction of the frequency trajectory with a total length of 5 ns. We also checked that the frequency correlation function is not affected by the transformation imposed by Eq. 7. The parameters of the correlation function were taken similar to simulations of the amide I frequency of N-methyl acetamide in acetonitrile [1], assuming that the dynamics of acetonitrile is not much different in these two systems. The slow correlation time was elongated to 3 ps to match echo-peak shift data on HDO dissolved in acetonitrile [2]. The frequency correlation functions of the upper local transitions were assumed to be identical to those used for the fundamental ones.

The magnitude and orientation of the local mode transition dipoles were fixed with the angle Θ between the two transition dipoles. This angle also determines the intensity ratio between the absorption from symmetric and asymmetric normal modes. Note that the fixed dipole orientations result in the lack of the true reorientational effects in the simulated spectra.

3.5 Discussion

The simulation procedure begins with modeling the linear absorption spectrum. It was recently shown [58] that the coupling is weakly solvent dependent. Therefore, we use the value derived from the linear spectrum of H_2O in acetonitrile. The coupling strength J was set at -35.6 cm^{-1} to match the splitting of the linear absorption spectrum into the symmetric and asymmetric modes. For the first approximation, the asymmetry parameter α was nullified, and the amplitude of the fluctuations σ was obtained from the linear spectrum ($\beta = 1$). The angle between the two dipole moments was set at 96^o to give the correct peak ratio in the absorption spectrum. The linear absorption spectrum is not very sensitive to the particular parameters of the correlation function; however, the fast correlation time was at the edge of the motional narrowing regime. With this in hand, the asymmetry parameter value was obtained as $\alpha = 1$ to provide the best match with the experimental spectrum, and the final alignment of all other parameters was allowed.

With the given Hamiltonian the average frequencies for the symmetric |100> and asymmetric |001> stretch vibrations are 3541 and 3613 cm^{-1}, respectively. The dashed line in Fig. 3.2(b) shows the calculated spectrum for H_2O diluted in acetonitrile, which was

Parameter	Value	Physical meaning	Obtained from
$<\omega>$	3773 cm^{-1}	Peak position	Absorption spectrum
J	-35.6 cm^{-1}	Peak splitting	-- //--
σ	58 cm^{-1}	Spectrum broadening	-- //--
Θ	96^{O}	Peak ratio	-- //--
α	1	Spectrum asymmetry	-- //--
β	0.517	Spectrum broadening	-- //--
T_F	150 fs	Fast environmental fluctuations	Ref.:[1,2]
T_S	3 ps	Slow environmental fluctuations	-- //--
A_F	0.85	Amplitude of fast fluctuations	-- //--
A_S	0.15	Amplitude of slow fluctuations	-- //--
Δ	210 cm^{-1}	Excited state absorption position	HDO: acetonitrile pump-probe[2]
d_{12}	1.3	Excited state absorption amplitude	H_2O: acetonitrile pump-probe

Table I. The parameters used in modeling.

obtained by averaging over 10 000 simulations equally spaced along the frequency trajectory. The values for all the parameters are summarized in Table I. Note that the absorption spectrum peak splitting of ~80 cm^{-1} is slightly larger than the expected value of $\sim 2J = 71.2$ cm^{-1} due to the peak spectral wings. The essential features of the absorption spectrum are nicely captured, especially considering the limitations of the model. Nonetheless, the symmetric band seems to be slightly narrower than the asymmetric one, while the calculated procedure yields identical widths as the two modes are treated at the same ground. The required width difference might potentially originate from the time dependence of the coupling constant *J*. The correctness of this assumption is beyond the capability of the pump-probe technique and can be potentially verified by 2D IR spectroscopy [14,38] and/or MD simulations. Anyhow, because of the lack of such data we do not pursue this issue further on.

With most of the parameters of the model fixed from the linear absorption spectrum, we can test the prediction power of the model for nonlinear spectroscopy. The anharmonicity constant for individual OH oscillators, $\Delta = 210$ cm^{-1}, was straightforwardly obtained from pump-probe measurements on HDO in acetonitrile [2]. This value is also close to that found from theoretical investigations [55,59] and nonlinear experiments [2,42] on the HOD dissolved in D_2O. Thus, only one still unknown parameter that is needed is the dipole moment of the doubly excited states, d_{12}.

The pump-probe spectrum was obtained by first calculating the relevant third-order response functions for a fixed waiting time using Eq. (11) of Ref. [53]. This was done

similarly to the linear absorption calculations using 10 000 starting points from the 5 ns Hamiltonian trajectory. The third-order response functions in the time domain for parallel and orthogonal pump-probe polarizations were then Fourier transformed along the time axes corresponding to the first and the last delays to give the 2D IR spectrum. The calculations of one 2D pattern typically took ~100 hours of computation time of one node of a 200 node cluster computer (the Rekencentrum of the Rijksuniversiteit Groningen). The pump-probe spectrum was obtained by integrating over the frequency corresponding in the time domain to the first time delay (the so-called excitation frequency [60]). This gives the pump-probe spectrum under the assumption of impulsive excitation. To account for the final pump pulse duration, the 2D pattern was normalized along the pump frequency axis onto the excitation spectrum [61].

The transient isotropic spectrum, calculated at 500 fs delays, is presented as a solid line in Fig. 3.3(b). The transition dipoles from the localized singly excited states to the doubly excited states were taken to be 1.3 times the transition dipole from the localized ground state to the singly excited states. This is slightly lower than the value of $\sqrt{2}$ for a harmonic potential, but close to that found in simulation studies [59]. The agreement of the calculated spectrum with its experimental counterpart is quite satisfactory considering the fact that only one parameter, d_{12}, was fitted.

The calculated frequencies for the symmetric |200> and asymmetric |002> stretch overtones and the combination band |101> are 6936, 7181, and 6965 cm^{-1}, respectively. In pump-probe spectra, bleaching and stimulated emission appear at the fundamental frequencies, and excited state absorption emerges at the six transition frequencies between the singly and doubly excited states (Fig. 3.1). The average frequencies for these transitions

	$\|000\rangle$	$\|200\rangle$	$\|101\rangle$	$\|002\rangle$
$\|100\rangle$	3541 (0.94 x)	3395 (-0.35 x)	3425 (-0.22 y)	3640 (-0.10 x)
$\|001\rangle$	3613 (1.00 y)	3323 (-0.10 y)	3352 (-0.24 x)	3568 (-0.59 y)

Table II: The calculated transition frequencies (in cm^{-1}) in the stretching mode region. The numbers in parentheses are the relative transition intensities and the transition dipole directions with the x-axis oriented along the C_2 axis and the z axis out of the molecular plane. The numbers are given for the asymmetry parameter $\alpha = 0$ and scaling coefficient $\beta = 1$.

are given in Table II and are shown as vertical lines in Fig. 3.3(b). However, these lines are hardly recognizable in the transient spectra because the peak separation is smaller than their widths. Therefore, the rich structure that includes in total eight transitions of different signs and dipole moment orientations are mostly hidden due to environmental fluctuations. This is especially true for the excited state absorption around 3380 cm^{-1}, whose broad structure cannot be resolved experimentally.

The isotropic transients exhibit little dynamics in the first 500 fs [Fig. 3.3(a)], which is consistent with an 8 ps lifetime. However, there is a noticeable intensity redistribution most clearly observed experimentally in the orthogonal pump and probe polarization configuration [Fig. 3.3(a), inset]. In contrast, the anisotropy is strongly frequency and delay dependent (Figs. 3.4 and 3.5). Within 500 fs, the anisotropy quickly decreases to values of 0.1-0.2 with the zero magnitude near the frequency of the $|001> \rightarrow |002>$ transition. The breaking point around 3470 cm^{-1} results from the progressive decrease of accuracy of the anisotropy calculations as the denominator [i.e., isotropic signal, Fig. 3.3(b)] approaches zero. The agreement with the experiment is quite good and the main features are well reproduced.

Figure 3.5(c) shows the calculated anisotropic transients at the same frequencies as the experimental ones shown in Figs. 3.5(a) and 3.5(b). The initial anisotropy is generally lower than the 0.4 value expected for a single-dipole transition. This is due to the interference of responses of overlapping transitions with different symmetries. For instance, the excitation of the symmetric mode depletes the population of the ground state, causing bleaching at the frequency of the asymmetric mode. The excited water molecules have a preferential orientation of the symmetric mode, leaving the "hole" in the ground state of the same orientation. However, this orientation is orthogonal to the asymmetric mode, hereby yielding an additional contribution to the orthogonally polarized pump-probe measurement. As a result, the initial anisotropy value is lower than the common 0.4 value characteristic of a single-dipole transition. This effect is the best seen at the 3625 cm^{-1} transient [Fig. 3.5(a)]. Similarly, the interference of the lower and higher-state transitions results in a short time value of anisotropy at the 3575 cm^{-1} transient. However, it should be noticed that the effect of the overlapping transitions alone is not sufficient to account for the observed subpicosecond anisotropy decay [Fig. 3.5(c)].

The short time dynamics are very similar to the ones observed in the experiment, with the substantial initial drop in the anisotropy. Around the frequency of the symmetric mode (3525 cm^{-1}), both the experiments [Fig. 3.5(a), green squares] and the calculations [Fig. 3.5(c), green curve] reach the zero value at 200 fs. Note that the reorientational motion of the molecule has not been included into the simulations, which proves that the observed anisotropy decays are solely due to *intramolecular* processes.

An interesting feature clearly seen in the anisotropy spectra at all frequencies in calculations and at some (i.e., 3525 and 3575 cm^{-1}) in experiment is an oscillatory component with the first recurrence at ~350 fs and quickly dampening. The model calculations from the time evolution operator (Eq. 3) demonstrate that these are damped Rabi oscillations with a decay that originates from decoherence imposed by the frequency fluctuations. While general signatures of this process are observed in experimental transients [Fig. 3.5(a)], the damping factor is higher than predicted theoretically. Potentially, such increased damping could arise from the finite probe pulse duration used in the experiments, whereas the calculations were made assuming delta pulses. However, with 70 fs pulses one would not expect substantial smearing of the oscillations with a period of 350 fs. Most likely, the assumption of totally uncorrelated frequency fluctuations of the two oscillators in Eq. 1 is not completely fulfilled as it has been demonstrated, for instance, in the case of rhodium dicarbonyl (RDC) complexes dissolved in hexane and chloroform [38]. Also, the coupling constant *J* might exhibit some time dependence. In either case, the pump-probe spectroscopy does not seem able to provide more information that has already been extracted.

In the impulsive pump-probe experiment, coherent excitation contributions and the population transfer between the symmetric and asymmetric modes are added up and cannot be easily separated. Since the transition dipoles for the symmetric and asymmetric stretch vibrations are almost perpendicular, the coherent excitation that requires a simultaneous excitation of the two orthogonal vibrations does not contribute greatly to the isotropic response. If the transition dipole moments are equal, the contributions of different terms can be estimated using the orientational averaging coefficients between the molecule and laboratory frame [62]. The ground-state bleach contributes 2/11 of the signal, the population transfer part of the stimulated emission contributes 6/11 of the signal, and the coherent excitation pathways contribute the remaining 3/11. Therefore, the anisotropy cannot decay to values below 8/11 of its initial value (i.e., below 0.29) without involving either substantial rotational motion or population transfer. As the former has been shown not to occur on a 0.5 ps time scale, the latter should contribute substantially to the anisotropy transients at short delays. We believe that more powerful 2D correlation experiments [38] that are already underway will shed some light on the interplay of coherence response versus population transfer.

3.6 Conclusions

In this chapter, the results of FTIR and IR pump-probe experiments on the stretching mode of water diluted in acetonitrile have been presented. The uniqueness of this system stems from the fact that H_2O molecules form reasonably strong hydrogen bonds to acetonitrile, but no extensive 3D hydrogen-bond network is established. This allows investigating the intramolecular processes and their manifestation in spectroscopic observables without complications imposed by many-body effects.

The FTIR spectroscopy on H_2O:acetonitrile and HDO:acetonitrile mixtures allowed us to identify symmetric and asymmetric modes of the H_2O molecule that appear due to the intramolecular coupling. The pump-probe spectroscopy revealed bleaching around the same frequencies as well as broad featureless induced absorption at ~3370 cm^{-1}. The isotropic component of the pump-probe signals show the frequency-independent 8 ps decay time that was ascribed to the stretching mode lifetime. At short times, extremely fast dynamics occurring with a 0.2 ps characteristic time have been observed.

The anisotropy demonstrates rich frequency-dependent dynamics with the dominant component at the 200 fs time scale. First, within the initial 500 fs the anisotropy decays to the values of ~0-0.2 depending on the probe frequency. Second, strongly damped oscillations with a period of 350-400 fs have been observed in anisotropy transients at certain wavelengths. The initial anisotropy decay is followed by the 2.2 ps tail, which is similar to the already reported [2,52] time scales of the water rotational diffusion.

The experimental data have been successfully described theoretically within the framework of a simple model that includes intramolecular coupling, anharmonicity, and environmental fluctuations. It has been shown that the lower transitions results from frequency splitting of the coupled oscillators into the symmetric and asymmetric modes. The steady-state absorption spectrum has been used to obtain most of the model parameters, with which the pump-probe spectrum has been subsequently described fairly well. The overall anisotropy features observed in experiments have also been reproduced. This is a powerful confirmation of the model reliability, given the fact that anisotropy is a more sensitive parameter as compared to the isotropic signal. The theoretical model does not invoke any rotational diffusion or interaction between different water molecules. Therefore, the observed features have an intramolecular origin and arise from the coupling of the two OH oscillators. Note that without taking the intramolecular processes into consideration, the biphasic decay and specific frequency dependence of the anisotropy can be misinterpreted as reflecting real rotational diffusion times along different molecular axes.

It is interesting to project the theoretical approach presented in this paper to other H_2O systems, in particular to bulk liquid water. One of the most surprising facts regarding the subpicosecond dynamics in bulk water is the extremely fast anisotropy decay that occurs at a 100 fs time scale [12,36,63]. This has been conventionally ascribed to energy transfer from the initially excited to randomly oriented OH oscillators due to their high density in liquid H_2O. Even putting aside numerous complications which arise from the strong isotropic thermal components to the pump-probe signal[2,13,25,28,48], the possibility of the intramolecular mechanism of the anisotropy decay has never been thoroughly considered. Our results demonstrate that purely *intramolecular* processes in the hydrogen-bonded H_2O molecule cause similar effects on the spectroscopic observables as the intermolecular interactions. Potentially, the former can cause a complete anisotropy decay within 200 fs at particular frequencies, as is the case for the 3525 cm^{-1} transient shown with green squares in Fig. 3.5(a). Therefore, for any H_2O containing systems, including bulk liquid water, it appears essential to analyze the complete spectrotemporal anisotropy dependence instead of a limited spectral range. For bulk water, the presented model, with the parameters correspondingly adjusted, predicts the anisotropy decay with 100 fs time. Therefore, it might well be possible that the ultrafast anisotropy decay observed in bulk water is, at least partially, a result of an intramolecular process. In addition, the intramolecular energy redistribution between symmetric and asymmetric modes may promote a subsequent intermolecular transfer by optimizing the dipole alignment with respect to an accepting neighboring dipole. However, it should be stressed that the considerations above are rather speculative as it is not clear whether the outlined model is applicable to liquid water in the first place. In particular, the whole framework of symmetric and asymmetric eigenmodes is very questionable with respect to liquid water. To further clarify these possibilities, additional experimental and theoretical investigations of water clusters are required.

References:

[1] T.l.C. Jansen; J. Knoester, J. Chem. Phys. **124**, 044502 (2006).
[2] D. Cringus; S. Yeremenko; M.S. Pshenichnikov; D.A. Wiersma, J. Phys. Chem. B **108**, 10376 (2004).
[3] S.K. Pal; A.H. Zewail, Chem. Rev. **104**, 2099 (2004).
[4] J.Lin; I.A. Balabin; D.N. Beratan, Science **310**, 1311 (2005).
[5] M. Chaplin, Nature Reviews - Molecular cell biology **7**, 861 (2006).
[6] G.A. Jeffrey, *An Introduction to Hydrogen Bonding*, Oxford University Press, New York, (1997).
[7] F. Franks, *Water: a comprehensive treatise*, Plenum Press, New York, (1972).
[8] U. Emmerichs; S. Woutersen; H.J. Bakker, J. Opt. Soc. Am. B **14**, 1480 (1997).
[9] S. Yeremenko; A. Baltuska; F.d. Haan; M.S. Pshenichnikov; D.A. Wiersma, Opt. Lett. **27**, 1171 (2002).
[10] C.J. Fecko; J.J. Loparo; A. Tokmakoff, Opt. Commun. **241**, 521 (2004).
[11] J.B. Asbury; T. Steinel; C. Stromberg; S.A. Corcelli; C.P. Lawrence; J.L. Skinner; M.D. Fayer, J. Phys. Chem. A **108**, 1107 (2004).
[12] M.L. Cowan; B.D. Bruner; N. Huse; J.R. Dwyer; B. Chugh; E.T.J. Nibbering; T. Elsaesser; R.J.D. Miller, Nature **434**, 199 (2005).
[13] T. Steinel; J.B. Asbury; J. Zheng; M.D. Fayer, J. Phys. Chem. A. **108**, 10957 (2004).
[14] J.D. Eaves; J.J. Loparo; C.J. Fecko; S.T. Roberts; A. Tokmakoff; P.L. Geissler, Proc. Natl. Acad. Sci. **102**, 13019 (2005).
[15] J.J. Loparo; S.T. Roberts; A. Tokmakoff, J. Chem. Phys. **125**, 194521 (2006).
[16] J.J. Loparo; S.T. Roberts; A. Tokmakoff, J. Chem. Phys. **125**, 194522 (2006).
[17] S. Woutersen; U. Emmerichs; H.K. Nienhuys; H.J. Bakker, Phys. Rev. Lett. **81**, 1106 (1998).
[18] G.-G. Chang; T.-M. Huang; H.-C. Hung, Proc. Natl. Sci. Counc. ROC(B) **24**, 89 (2000).
[19] J.A. McGuire; Y.R. Shen, Science **313**, 1945 (2006).
[20] M. Smits; A. Ghosh; M. Sterrer; M. Muller; M. Bonn, Phys. Rev. Lett. **98**, 098302 (2007).
[21] T. Patzlaff; M. Janich; G. Seifert; H. Graener, Chemical Physics **261**, 381 (2000).
[22] G. Seifert; T. Patzlaff; H. Graener, Phys. Rev. Lett. **88**, 147402 (2002).
[23] J.C. Deak; Y. Pang; T.D. Sechler; Z. Wang; D.D. Dlott, Science **306**, 473 (2004).
[24] H.S. Tan; I.R. Piletic; R.E. Riter; N.E. Levinger; M.D. Fayer, Phys. Rev. Lett. **94**, 057405 (2005).

[25] D. Cringus; J. Lindner; M.T.W. Milder; M.S. Pshenichnikov; P. Vöhringer; D.A. Wiersma, Chem. Phys. Lett. **408**, 162 (2005).
[26] I.R. Piletic; D.E. Moilanen; D.B. Spry; N.E. Levinger; M.D. Fayer, J. Phys. Chem. A **110**, 4985 (2006).
[27] A.M. Dokter; S. Woutersen; H.J. Bakker, Phys. Rev. Lett. **94**, 178301 (2005).
[28] D. Cringus; A. Bakulin; J. Lindner; M.S. Pshenichnikov; P. Vöhringer; D.A. Wiersma, in preparation.
[29] H. Graener; G. Seifert, J. Chem. Phys. **98**, 36 (1993).
[30] H. Graener; G. Seifert; A. Laubereau, Chem. Phys. **175**, 193 (1993).
[31] J.J. Gilijamse; A.J. Lock; H.J. Bakker, PNAS **102**, 3202 (2005).
[32] D.L. Bergman; A. Laaksonen, Phys. Rev. E **58**, 4706 (1998).
[33] D.S. Venables; C.A. Schmuttenmaer, J. Chem. Phys. **113**, 11222 (2000).
[34] R.D. Mountain, J. Phys. Chem. A. **103**, 10744 (1999).
[35] I. Bako; T. Megyes; G. Palinkas, Chem. Phys. **316**, 235 (2005).
[36] S. Woutersen; H.J. Bakker, Nature **402**, 507 (1999).
[37] R.G. Gordon, J. Chem. Phys. **45**, 1643 (1966).
[38] M. Khalil; N. Demirdoven; A. Tokmakoff, J. Phys. Chem. A **107**, 5258 (2003).
[39] G. Herzberg, *Infrared and Raman spectra of polyatomic molecules*, Van Nostrand, New York, (1945).
[40] G.E. Walrafen, J. Chem. Phys. **48**, 244 (1968).
[41] J.R. Scherer; M.K. Go; S. Kint, J. Phys. Chem. **78**, 1304 (1974).
[42] C.J. Fecko; J.D. Eaves; J.J. Loparo; A. Tokmakoff; P.L. Geissler, Science **301**, 1698 (2003).
[43] L.F. Scatena; M.G. Brown; G.L. Richmond, Science **292**, 908 (2001).
[44] J.J. Loparo; A. Tokmakoff, (private communication).
[45] D. Cringus; M.S. Pshenichnikov; D.A. Wiersma, in preparation
[46] D. Laage; J.T. Hynes, Science **311**, 832 (2006).
[47] C.P. Lawrence; J.L. Skinner, Chem. Phys. Lett. **369**, 472 (2002).
[48] J. Lindner; P. Vöhringer; M.S. Pshenichnikov; D. Cringus; D.A. Wiersma; M. Mostovoy, Chem. Phys. Lett. **421**, 329 (2006).
[49] S. Ashihara; N. Huse; A. Espagne; E.T.J. Nibbering; T. Elsaesser, Chem. Phys. Lett. **424**, 66 (2006).
[50] S. Ashihara; N. Huse; A. Espagne; E.T.J. Nibbering; T. Elsaesser, J. Phys. Chem. A **111**, 743 (2007).
[51] G. Seifert; T. Patzlaff; H. Graener, J. Chem. Phys. **120**, 8866 (2004).
[52] J.J. Loparo; C.J. Fecko; J.D. Eaves; S.T. Roberts; A. Tokmakoff, Phys. Rev. B **70**, 180201 (2004).

[53] T.l.C. Jansen; J. Knoester, J. Phys. Chem. B. **110**, 22910 (2006).
[54] H. Torii, J. Phys. Chem. A. **110**, 4822 (2006).
[55] A. Piryatinski; C.P. Lawrence; J.L. Skinner, J. Chem. Phys. **118**, 9672 (2003).
[56] T. Hayashi; T.l.C. Jansen; W. Zhuang; S. Mukamel, **109**, 64 (2005).
[57] S. Mukamel, *Principles of Nonlinear Optical Spectroscopy*, Oxford University Press1999).
[58] G. Seifert; T. Patzlaff; H. Graener, J. Chem. Phys. **125**, 154506 (2006).
[59] T.l.C. Jansen; T. Hayashi; W. Zhuang; S. Mukamel, J. Chem. Phys. **123**, 114504 (2005).
[60] D.M. Jonas, Annu. Rev. Phys. Chem. **54**, 425 (2003).
[61] M.K. Yetzbacher; N. Belabas; K.A. Kitney; D.M. Jonas, J. Chem. Phys. **126**, 044511 (2007).
[62] R.M. Hochstrasser, Chem. Phys. **266**, 273 (2001).
[63] H. Torii, J. Phys. Chem. A. **110**, 9469 (2006).